SEMI-AUTOMATIC RECOGNITION OF LUNAR GEOLOGIC UNITS BASED ON TEXTURE AND SPECTRAL FEATURES USING IMAGE DATA OBSERVED BY KAGUYA, LISM TC/MI

Y. Shibata[1],N. Hirata[1], H. Demura[1], N. Asada[1], Y. Yokota[2], T. Morota[2], C. Honda[2], T. Matsunaga[3], M. Ohtake[2], J. Haruyama[2], [1]The University of Aizu, Ikki-machi, Aizu-Wakamatsu City, Fukushima 965-8580, JAPAN, [2]JAXA, [3]NIES

Introduction: Recognition of geologic units on image data is a fundamental analytical step of remote sensing. A single geologic unit could be defined as a region with its own particular features, which represent its origin. The same units have common photogeological characteristics. Criteria for determining the units are varied between previous and recent researches. In 1960's and 1970's, researchers in lunar science used panchromatic photographs to make lunar geologic maps. Their basic criteria of geologic units are defined by surface textures and topographic features in the photographs. Recently, variation of remote sensing data has greatly expanded. Resolution and coverage of image data are increase, and multi-spectral images of the moon have been obtained through modern lunar missions [1]. We especially focus on recognition of geologic units by combining texture and spectral features extracted from image data.

In addition, many techniques for automatic or semi-automatic image classification are developed. If these techniques are effective for recognition of geologic units in remote sensing data, automatic or semi-automatic data processing would be an important method for production of geologic maps of the moon. We have already presented the preliminary method for semi-automatic recognition of geologic units using image data of Apollo and Clementine [2]. The purpose of this research is to test the preliminary method with lunar high-resolution images and multi-spectral images obtained by Terrain Camera (TC) [3] and Multiband Imager (MI) [4] onboard the Kaguya lunar explorer.

Texture is controlled by surface undulation and reflectance of the object, and illumination conditions. While the surface undulation controls the texture at low solar elevations, the reflectance governs at high solar elevations. The variance of digital number of pixels in certain area is one of the statistical indices for texture features, and is adopted in this research.

Spectral features are representation of characteristics of reflectance spectra of materials. They are derived from image calculations of multi-spectral image data. Band ratio is widely utilized spectral features [5]. The band ratios are proxies of the slope of spectral continuum or the depth of absorption bands. For the lunar case, they represent the contents of mafic minerals and the degree of space weathering [6]. Absorption band depths are other possible spectral features, which are more direct representatives of the material type. K-means clustering algorithm is adopted to label pixels based on the both texture and spectral features in this research. The algorithm is one of the most popular methods for unsupervised image classification.

Method/Data: This research adopts following procedures as an experimental ones of the semi-automatic recognition; 1) The value of variance is derived as the texture feature using so-called filtering process whose shape of the filter is square, 2) The band ratios and the absorption band depths are derived as the spectral features, 3) The texture and spectral features are normalized to the interval [0, 1], 4) K-means clustering is applied for classification. Arbitrary number of texture feature maps and spectral feature maps are used as input data. We use high-resolution images (10m/pixel) observed by Terrain Camera (TC) and 9-band multi-spectral images (VIS: 20m/pixel, NIR: 62m/pixel) observed by Multi-band Imager (MI) as test data of the classification procedure. Fig. 1 is a single band image (750nm) observed by MI. This image shows the southern central area of the Orientale basin at 93°W, 24°S, and the image coverage is 20 x 122 km. We find a part of large basaltic deposits and highland in Orientale basin with many pristine impact craters. Three combinations of the MI band are adopted to take the band ratios: 750nm/415nm, 750nm/950nm, and 415nm/750nm. They are common sets for lunar multi-band images. The absorption depth at 900nm, 950nm, 1000nm, 1050nm and 1250nm are also extracted.

Results: Fig.2 shows a variance map derived from Fig.1. The window size is 21 x 21 pixel, corresponding 420 x 420 m in the real scale. Bright pixels represent high-variance regions and dark pixels are low-variance regions. Fig. 3 shows a false color image of the band ratios with the color assignment of R, G and B for 750/415 nm, 750/950 nm, and 415/750 nm, respectively. Fig. 4 shows a false color image of absorption depths with the color assignment of R, G and B for 950 nm, 1050 nm, and 1250 nm, respectively. Fig. 5 shows a result of k-means clustering of the variance map and the band ratio maps of 750/415 nm, and 750/950 nm. Fig. 6 shows a result of k-means clustering of the absorption depth map. The number of class is 5 in both clustering results, and each class is colored with different color.

Discussion and Summary: In Fig.2, distribution of large variance pixels (white) shows spotty squared patterns. It corresponds to location of pristine craters on the original 750nm image of MI (Fig. 1). In particular, the pattern is found in the lower three quarter part (highland) of the Fig. 2. In Fig. 3, the lower area shows redder than the upper quarter area (basaltic deposit). Therefore the lower highland and upper basaltic deposits are composed of different materials and they might be affected by space weathering. And, green components (750/950nm) in Fig. 3 show spotty pattern of large values in the upper basaltic deposit. In contrast, few spotty patterns of green components are found in the lower highland area. Therefore the upper basaltic deposit corresponds to the mafic-rich one. In Fig. 4, the lower highland area shows bluer than the upper basaltic deposit. Therefore the absorption depth at 1250nm in the lower area is deeper than that of the upper basaltic deposit. Yellow components (950nm and 1050nm) in Fig. 4 show large value in the upper basaltic deposit. Therefore the absorption depth at 950nm and 1050nm in the upper basaltic deposit is deeper than that of the lower highland area.

Figs. 5 and 6 are results of k-means clustering based on texture and spectral features. In Fig. 5, the class-1 (navy) and the class-2 (green) show the same pattern of large value in the variance map. The class-1 is located at the area of largest variance (Fig. 2) and at pristine craters (Fig. 1). The class-2 matches the area of the larger variance area (Fig. 2). On the other hand the class-3 and 4 (blue and yellow) are mafic-rich area because large value of green component (750/950nm) in Fig. 3 corresponds to these two classes. The class-5 (red) is the mafic-poor area because the green component (750/950nm) is small in Fig. 3. In Fig. 6, the class-1 (navy), the class-2 (green) and the class-5 (red) show the same pattern of large value of blue components (1250nm) in absorption depth map. On the other hand, the class-4 (yellow) corresponds to yellow component (950nm and 1050nm) in Fig. 4. The class-3 (blue) matches the area that shows deep absorption at 950nm, 1050nm and 1250nm because the class corresponds to white spotty pattern in Fig. 4.

This research showed first step for semi-automatic recognition by means of ongoing KAGUYA data.

References: [1] S. Nozette. et al. (1994) *Science, 266,* 1835-1839 [2] Y. Shibata. et al. (2008) *LPS XXIX*, Abstract #1234 [3] J. Haruyama. et al. (2008) *Earth Planets Space, 60,* 243-255 [4] M. Ohtake. et al. (2008) *Earth Planets Space, 60,* 257-264 [5] C. M. Pieters. et al. (1994) *Science, 266,* 1844-1847 [6] C. M. Pieters. et al. (2000) *Meteoritics and Planet. Sci., 35,* 1101-1107.

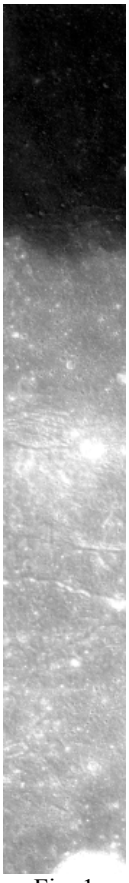

Fig. 1
MI 750nm-band image

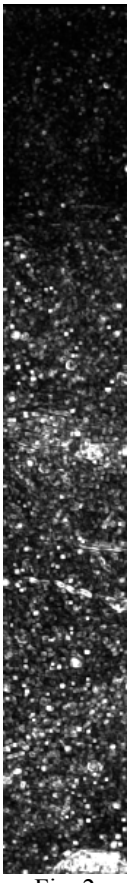

Fig. 2
Texture map (Variance)

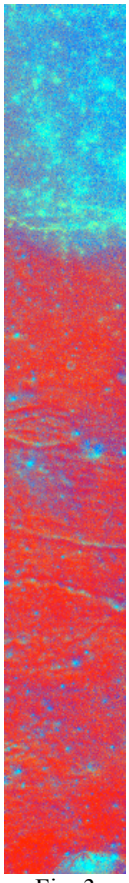

Fig. 3
Spectral map (Band ratio)

Fig. 4
Absorption depth map

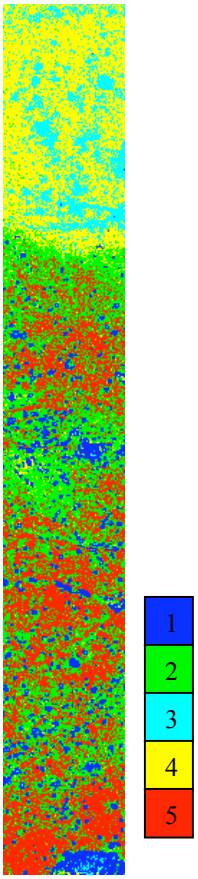

Fig. 5
K-means Classification map A

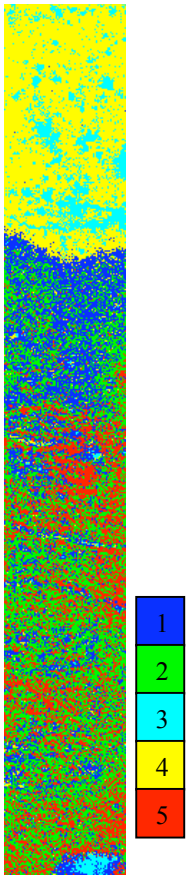

Fig. 6
K-means Classification map B